Journal of Applied Polymer Science

Effect of an alkalized-modified halloysite on PLA crystallization, morphology, mechanical, and thermal properties of PLA/halloysite nanocomposites

Jianhua Guo,[1] Junxia Qiao,[1] Xin Zhang[2]

[1]School of Materials Science and Engineering, South China University of Technology, Guangzhou 510640, China
[2]Department of Physics and Optoelectronic Engineering, Guangdong University of Technology, Guangzhou 510006, China
Correspondence to: J. H. Guo (E-mail: psjhguo@scut.edu.cn) and X. Zhang (E-mail: xinxintwinkle@126.com)

ABSTRACT: Poly(lactic acid) (PLA)/alkalized halloysite nanotube (HNTa) nanocomposites were prepared by melt mixing. The morphology, crystallization behavior, mechanical properties, and thermal stability of the nanocomposites were investigated in comparison with those of the pristine PLA. HNTa can nucleate PLA, leading to a lower recrystallization temperature and higher crystallinity. Infrared spectra revealed that the hydroxyl groups of the PLA interacted with the external hydroxyl groups of HNTa nanofillers via hydrogen bonding. The thermal stability of the nanocomposites was improved with the addition of HNTa. The PLA/HNTa nanocomposites exhibited higher modulus and tensile strength than those of the PLA composites containing unmodified halloysite nanotubes (HNTs). The improvement in properties was probably due to a better dispersion of the HNTa in the PLA matrix compared to that of the unmodified HNTs. Therefore, the facile alkali treatment of HNTs offers a low cost nanofiller for the preparation of PLA based nanocomposites with high tensile modulus and tensile strength. © 2016 Wiley Periodicals, Inc. J. Appl. Polym. Sci. **2016**, *133*, 44272.

KEYWORDS: crystallization; halloysite; mechanical property; morphology; poly(lactic acid); thermal stability

Received 11 May 2016; accepted 2 August 2016
DOI: 10.1002/app.44272

INTRODUCTION

Biodegradable poly(lactic acid) (PLA) is receiving much attention for various utilizations, such as packaging, biomedical applications, textiles, and certain engineering applications.[1–3] Many attempts have been made to tailor the properties of PLA by combining it with different dispersed phases such as micro- and nano-fillers, flame retardants and thermal stabilizers for many specific applications.[4–6]

Notably, PLA has been combined with various nanofillers such as organo-modified layered silicates, α-Zirconium phosphate, carbon nanotubes (CNTs), graphite derivatives, zinc oxide, and silver nanoparticles to improve various physiochemical properties including stiffness, flame retardancy, thermal stability, electrical conductivity, crystallization behavior, and antibacterial performance.[7–14]

Some two-dimensional nanofillers, such as montmorillonite (MMT), graphene, and α-Zirconium phosphate, have been widely utilized to prepare various polymer composites for packaging applications due to their excellent improvement in mechanical, thermal, and gas barrier properties.[15,16] Among them, MMT is probably the most popular nanofiller. However, MMT needs to be exfoliated before being incorporated into a polymer matrix, which translates to additional processing cost and time. Graphene is known for its exceptional mechanical properties and high aspect ratio. However, due to its high price, it is impractical to adopt graphene into conventional packaging materials at this stage.

Halloysites (HNTs) consist of 1:1 aluminosilicate layers with a tubular structure.[17] They have advantages including easy dispersion in aqueous and organic solvents after being dried. HNTs are non-toxic and durable in high shear mixing.[18] HNTs are available in large quantities, so they are much more affordable than CNTs and graphene. As a result, HNTs have recently received considerable attention for enhancing various physical properties of different polymers, including PLA,[19] polypropylene,[20] chitosan,[21] polyethylene terephthalate,[22] polyamide,[23] ethylene-propylene-diene monomer,[24] and diene rubber[25], etc.

However, there still remain some challenges in the utilization of HNTs for PLA based composites. First, HNTs tend to agglomerate into clusters during the preparation of nanocomposites. Second, the interfacial adhesion of HNTs and PLA is not ideal because of the low concentration of hydroxyl groups on the external surface of unmodified HNTs. To increase the concentration of hydroxyl groups on the external surface of HNTs, Zeng *et al.*[26] developed a facile NaOH treatment with HNTs.

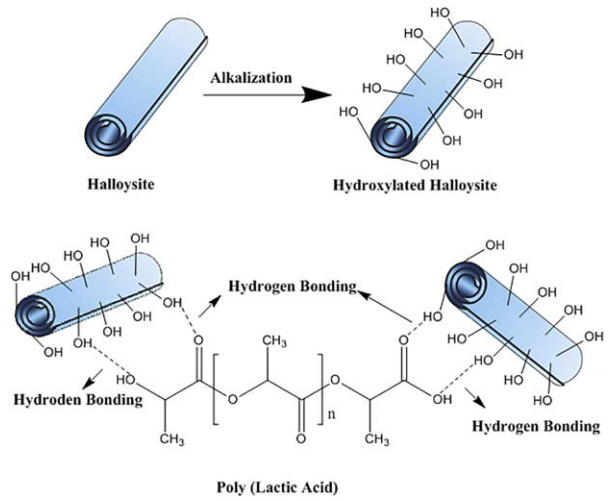

Figure 1. The procedure of HNT alkalization and the schematic illustration of hydrogen bonding between alkalized HNT and poly (lactic acid). [Color figure can be viewed at wileyonlinelibrary.com.]

It was shown that the alkalized HNT could be uniformly dispersed in an epoxy resin matrix, which led to considerable enhancement in both the stiffness and the toughness of the resultant nanocomposites.

In this report, the crystallization, morphology, mechanical properties, and thermal stability of PLA/HNT nanocomposites were investigated to determine the effect of the surface treatment and use of alkalized HNTs on the key characteristics of PLA.

EXPERIMENTAL

Materials

Extrusion grade poly(lactic acid), PLA 4043D, was supplied by NatureWorks LLC with a density of 1.24 g/cm^3. Halloysites (HNTs) in a powdered form were obtained from Applied Minerals, Inc. The halloysites have a length in the range of 0.5–3.0 microns, an exterior diameter in the range of 50–70 nanometers and an internal diameter (lumen) in the range of 15–30 nanometers. Sodium hydroxide was ordered from VWR International. All the other chemicals were used as received without further treatment.

Table I. Sample Composition and Symbols

Sample composition (wt %)	Sample symbol
Pristine PLA (reference)	PLA
PLA/HNT (99/1)	1PHNT
PLA/HNT (96/4)	4PHNT
PLA/HNT (93.5/6.5)	6.5PHNT
PLA/HNT (91/9)	9PHNT
PLA/HNTa (99/1)	1PHNTa
PLA/HNTa (96/4)	4PHNTa
PLA/HNTa (93.5/6.5)	6.5PHNTa
PLA/HNTa (91/9)	9PHNTa

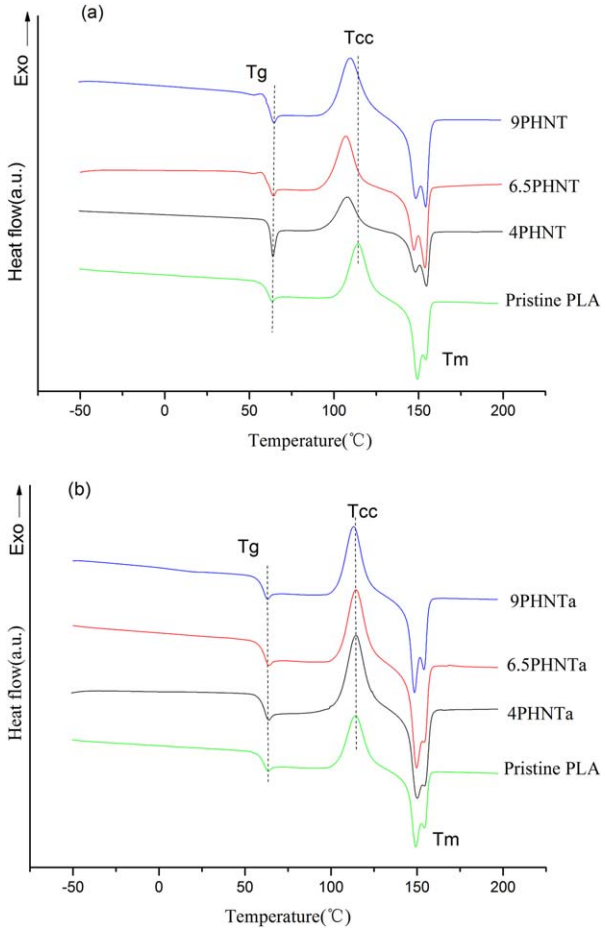

Figure 2. The second heating DSC curves of the nanocomposites: (a) pristine PLA and PLA/HNT nanocomposites; (b) pristine PLA and PLA/HNTa nanocomposites. [Color figure can be viewed at wileyonlinelibrary.com.]

The HNT was surface treated by NaOH following the method reported in the literature,[26] and are referred to as alkalized halloysite nanotube (HNTa). The procedure of HNT alkalization and the proposed interaction between the HNTa and PLA are shown in Figure 1. Many hydroxyl groups appeared on the external surface of the HNT after alkalization, which can be testified by XPS analysis.[26] Then, hydrogen bonding occurred between HNTa and PLA molecules in PLA and HNT composites.

Preparation of Nanocomposites

Before processing, PLA was dried at 80 °C for 12 h under vacuum. To minimize the water content for melt blending with PLA, the nanofillers were dried at 100 °C for 24 h and then were used directly for melt compounding. The nanofillers were melting mixed together with PLA at 180 °C by using a mini extruder (HAAKE Minilab II Micro Compounder, Karlsruhe, Germany). The PLA and HNT (or HNTa) were mixed at 50 rpm speed and 180 °C. The PLA and HNT (or HNTa) were mixed at 50 rpm speed and 180 °C. The loading of HNT (or HNTa) nanofillers are 1, 4, 6.5, and 9 wt %, respectively. For comparison, pristine PLA was processed under the same condition. All the samples and their symbols are summarized in Table I.

Table II. DSC Data (The Second Heating, 10 °C/min) of PLA, PLA/HNT Nanocomposites, and PLA/HNTa Nanocomposites

Entry	Sample code	T_g (°C)	ΔH_{rel} (J/g)	T_{cc} (°C)	ΔH_{cc} (J/g)	T_m (°C)	ΔH_m (J/g)	X_c (%)
1	PLA	63.1	2.4	110.4	24.5	149.5, 154.6	29.7	5.5
2	4PHNT	63.8	2.5	107.7	23.6	148.0, 154.2	28.5	5.2
3	6.5PHNT	64.6	2.3	107.6	23.3	147.6, 153.8	28.6	5.7
4	9PHNT	64.5	2.1	107.9	21.9	148.6, 153.2	28.1	6.7
5	4PHNTa	63.4	2.2	110.2	25.7	147.2, 153.4	32.5	7.3
6	6.5PHNTa	64.0	2.0	109.5	24.3	148.6, 153.9	31.5	7.7
7	9PHNTa	64.7	2.0	109.2	23.7	147.2,153.9	31.7	8.6

Nanocomposite plaques were prepared by a mini injector (HAAKE MiniJet Pro Piston Injection Molding System, Karlsruhe, Germany) with a width of ca. 5.0 mm and a thickness of ca. 1.7 mm.

Characterization

Thermogravimetric analyses (TGA) were performed by using a TA Instruments thermogravimetric analyzer (TGA Q500). The samples were heated from 25 to 700 °C at a rate of 10 °C/min under nitrogen flow.

Differential scanning calorimetry (DSC, Q100 from TA Instruments) characterizations were performed under nitrogen flow at a rate of 10 °C/min from −50 to 200 °C. The samples were kept at 200 °C for 3 min to eliminate the thermal history before they were cooled down to −50 °C at ramping rate of 10 °C/min. Then the samples were again heated to 200 °C at ramping rate of 10 °C/min. The glass transition temperature (T_g), enthalpy of relaxation (ΔH_{rel}), cold crystallization temperature (T_{cc}), enthalpy of cold crystallization (ΔH_{cc}), melting temperature (T_m), and melting enthalpy (ΔH_m) were evaluated. The degree of crystallinity (X_c) was determined by subtracting ΔH_{cc} from ΔH_m, and 93 J/g[27] was considered the melting enthalpy for 100% crystalline PLA.

Tensile tests were performed using an Instron Dynamometer (5869 model) under a crosshead speed of 50 mm/min. The sample dimensions were 50 mm × 5 mm × 1.68 mm. The distance between the grips was 20 mm.

X-ray diffraction characterization (XRD) was performed with a D5000 Theta diffractometer with Ni-filtered Cu Kα radiation (λ = 1.54056 Å) at room temperature. For Fourier Transform Infrared Spectroscopy (FT-IR) analysis, IR spectra were recorded on a Nicolet MEGNA IR 560 spectrophotometer with a Specac-Quest Diamond Attenuated Total Reflection (ATR) accessory. Nanocomposite samples were characterized in the ATR mode using sheet specimens. HNTs were mixed and pelleted with KBr for FT-IR characterization. Thirty-two consecutive scans from 4000 to 400 cm^{-1} were taken with a wavenumber resolution of 2 cm^{-1}.

Scanning electron microscopy (SEM) was used to image the fracture surfaces of the PLA and PLA based nanocomposites. The fracture surfaces were prepared by snapping specimens in a liquid nitrogen environment. The fracture surfaces were then sputter-coated with a thin layer of gold before the SEM imaging using a LEO1530 VP scanning electron microscope.

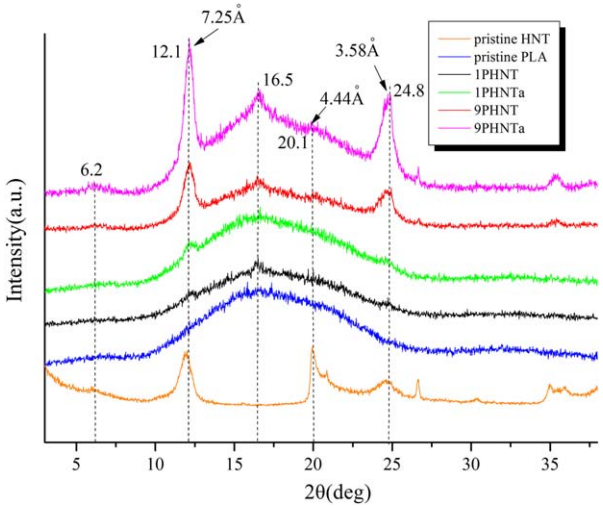

Figure 3. XRD patterns of PLA, HNT, PLA/HNT nanocomposites, and PLA/HNTa nanocomposites. [Color figure can be viewed at wileyonlinelibrary.com.]

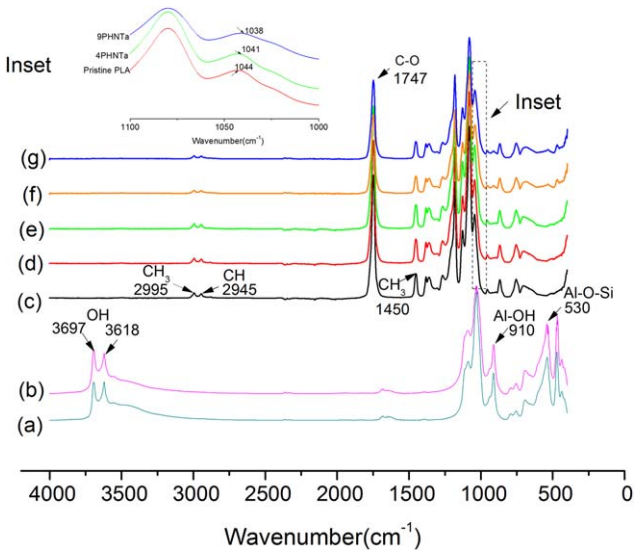

Figure 4. FT-IR spectra of pristine PLA, nanofillers and nanocomposites: (a) HNT, (b) HNTa, (c) PLA, (d) 4PHNT, (e) 4PHNTa, (f) 9PHNT, (g) 9PHNTa. [Color figure can be viewed at wileyonlinelibrary.com.]

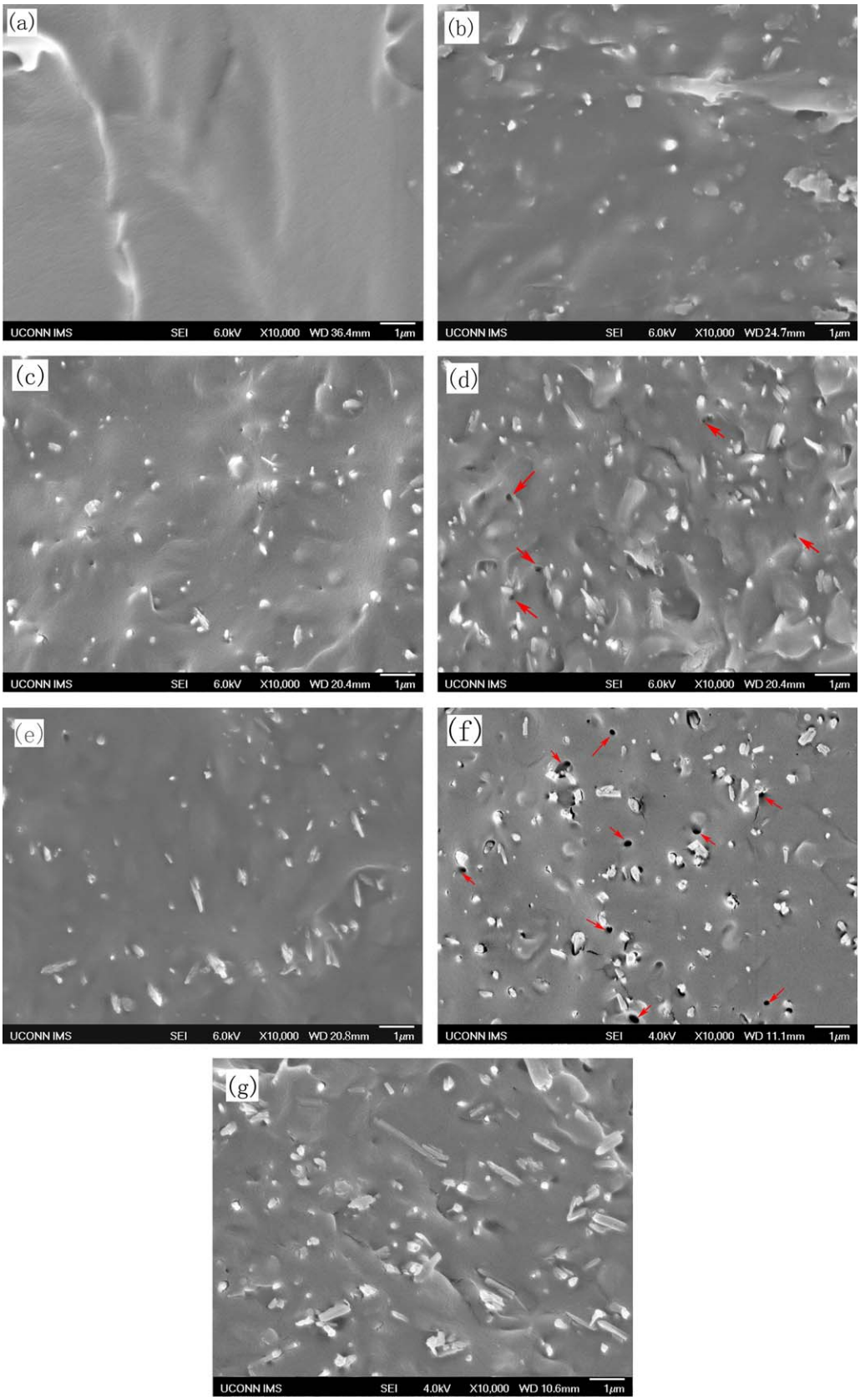

Figure 5. Fracture surface morphology of (a) pristine PLA, (b) 4PHNT, (c) 4PHNTa, (d) 6.5PHNT, (e) 6.5PHNTa, (f) 9PHNT, (g) 9PHNTa nanocomposites. [Color figure can be viewed at wileyonlinelibrary.com.]

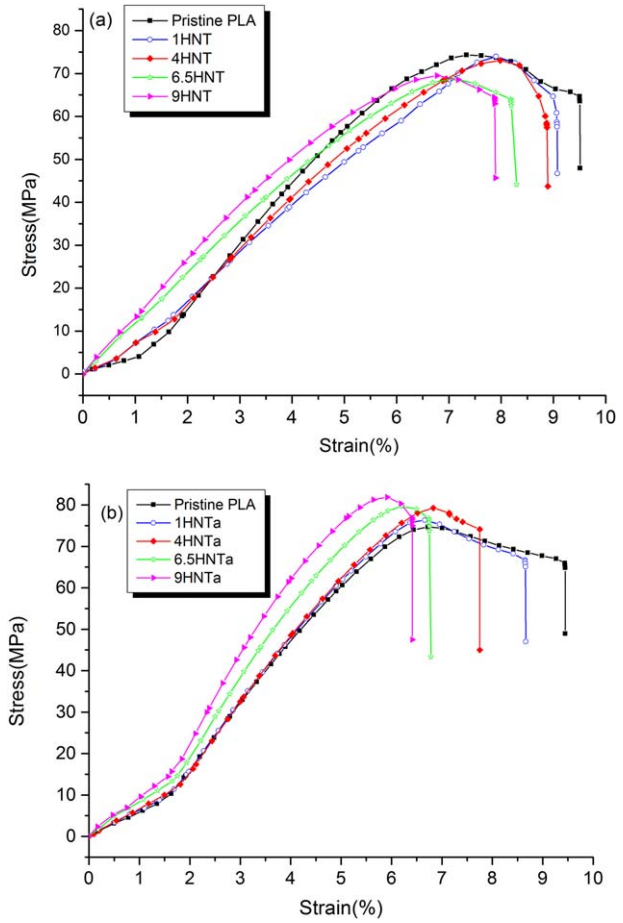

Figure 6. Stress-strain curves of (a) pristine PLA and PLA/HNT composites, (b) pristine PLA and PLA/HNTa composites. [Color figure can be viewed at wileyonlinelibrary.com.]

RESULTS AND DISCUSSION

Crystallinity

The quantification of PLA crystallinity was carried out by DSC and XRD. Figure 2 shows the second heating DSC thermograms of the nanocomposites compared to those of the pristine PLA. The detailed results are summarized in Table II.

The calorimetric data show that all the samples exhibited evident crystallization exotherms, which suggests that the starting materials possess a low crystallinity or amorphous structure. Then, the endothermic enthalpy of relaxation (ΔH_{rel}) shows only minor variety with various nanofiller loadings. The enthalpic relaxation is exclusively related to the amorphous phase of the polymer, which is typical for PLA in the glassy state undergoing some physical aging.[28] The T_g of the PLA/HNT and PLA/HNTa nanocomposites increased slightly with an increasing loading of HNT or HNTa, respectively, which could be attributed to the formed hydrogen bonding between the nanofillers and PLA. The cold crystallization peak of PLA (T_{cc}) shifted to a lower temperature with the addition of HNT or HNTa (Table II). This could be ascribed to the nucleating effect of HNT in the PLA cooling crystallization process. The melting temperatures of the PLA based nanocomposites are slightly lower than that of the pristine PLA. As HNT acted as a nucleating agent of PLA, the PLA/HNT nanocomposites can crystallize more quickly than the pristine PLA.[19] As a consequence, the melting temperature of nanocomposites was lower than that of pristine PLA. A similar phenomenon was also observed in PLA/CNT[29] and PLA/silica nanocomposites.[30] The multiple T_m peaks on the DSC thermograms can be ascribed to the melting of the crystalline regions of various sizes and perfection formed during the cooling and crystallization processes. The crystallinities (X_c) of the PLA/HNT nanocomposites were higher than that of the pristine PLA, and X_c increased with an increasing concentration of HNT or HNTa. Moreover, the PLA/HNTa nanocomposites exhibited a higher X_c than the PLA/HNT nanocomposites with the same loading of nanofillers, which is ascribed to the better dispersion of alkalized HNT in the PLA matrix. Based on the above results showed that the nanocomposites possessed a mainly amorphous structure (low crystallinity), which is also supported by the XRD results.

Figure 3 shows the XRD patterns of pristine PLA, pristine HNT, PLA/HNT nanocomposites, and PLA/HNTa nanocomposites. The pristine PLA and the nanocomposites show a broad hump at approximately $2\theta = 16.5°$, indicating mainly an amorphous structure.[10] The nanocomposites filled with both HNT and HNTa can be considered mainly amorphous, or only with a low crystallinity, because no diffraction peaks were shown in the XRD patterns. Moreover, the diffraction peaks evidenced at $2\theta = 12.1°$, 20.1°, and 24.8° are characteristic for halloysites and are ascribed to (001) (020) and (002) reflection planes, respectively,[31,32] whereas their intensity is increasing with an increased loading of nanofillers. The diffraction peaks at $2\theta = 16.5°$ of the 9PHNTa composites show more significant intensity than that of the 9PHNT composites, which indicates that the HNTa is beneficial to the crystallization of the PLA.

Ft-IR

The FT-IR spectra of the pristine PLA, HNT, HNTa, and their composites are shown in Figure 4. FT-IR spectra of HNT and HNTa [Figure 4(a,b)] exhibited two characteristic bands at around 3618 and 3697 cm^{-1}, which were assigned to the vibration of the inner hydroxyl groups and the hydroxyl groups located at the octahedral surfaces of the nanofillers, respectively.[33] The absorption bands at 2995 and 2945 cm^{-1} are arising from the C—H stretching vibrations of CH_3 and CH groups. Also in the spectrum for PLA, the stretching vibration of C—O groups is located at 1747 cm^{-1}, the bending vibration of CH_3 groups at 1450 cm^{-1}, and absorption bands at 1384 cm and 1364 cm^{-1} are arising from the C—H deformation and asymmetric/symmetric bending, respectively.[34] In this region, the intensities and the position of the PLA characteristic peaks did not change significantly with the addition of HNTs. For the spectrum for the PLA/HNT nanocomposites, in the region of 1300–500 cm^{-1}, the characteristics absorption bands of HNT and PLA were overlapped. For example, the main absorbance bands at 1094 and 1029 cm^{-1} associated with the stretching of the Si—O—Si bonds of HNT were overlapped by the bands at 1091 and 1043 cm^{-1} of the C—O—C and C—CH_3 bonds of PLA.[19] Therefore, it was hard to discriminate the changes of the bands for these samples in this region. In the spectra of HNT or HNTa, the absorption bands at 530 and 910 cm^{-1} were associated with the deformation of the Al—O—Si

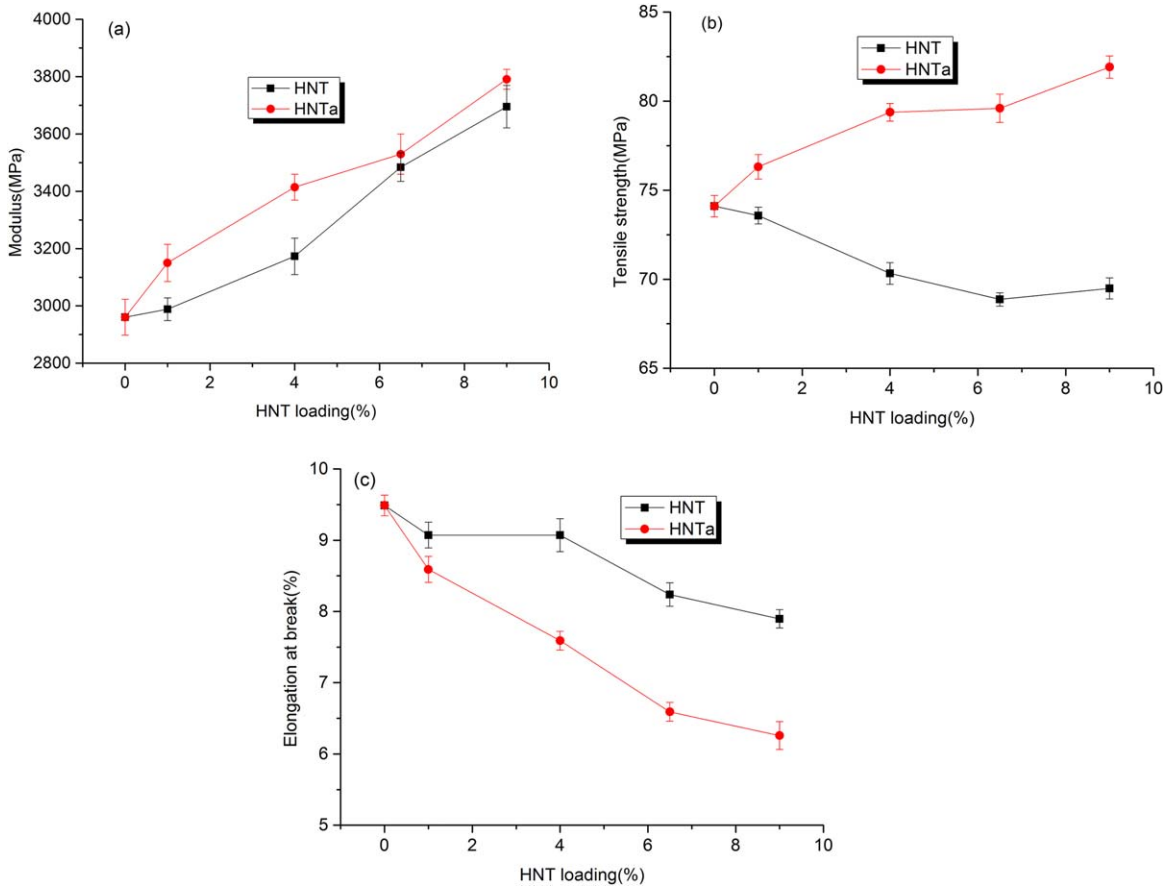

Figure 7. Tensile properties of PLA/HNT composites and PLA/HNTa composites (a) elastic modulus; (b) tensile strength; (c) elongation at break. [Color figure can be viewed at wileyonlinelibrary.com.]

and Al—OH groups, respectively. The elaborated part in Figure 4 within the range of 1110–1000 cm^{-1} (inset) shows the FT-IR spectra of pristine PLA, 4PHNTa composite, and 9PHNTa composite. In the spectra of the PLA and HNTa composites, a shift was observed for the absorption band at 1043 cm^{-1}, which is associated with the vibration peak of C—CH_3 of the PLA. This shift to a lower wavenumber with increasing HNTa content could be attributed to the hydrogen bonding interactions between HNTa and PLA. The hydrogen bonding interactions between PLA and HNT nanofillers were also confirmed by FT-IR analysis in the research of Silva[8] about PLA and halloysite films. A similar red shift peak at 1031 cm^{-1} appears, which implies the external surface of Si—O groups could form a hydrogen bonding with PLA.

Morphological Analysis

The fracture surface morphology of the PLA/HNT and PLA/HNTa nanocomposites is shown in Figure 5. It is shown that the morphology of pristine PLA [Figure 5(a)] is quite smooth. An appreciable increase in the number of micro voids [Figure 5(d,f), as marked by arrows] was observed with an increasing HNT concentration. Much more voids were observed in the 9PHNT composites than those in the 9PHNTa nanocomposites, which implies that unmodified HNTs tend to be aggregated in the PLA matrix and are much easier to detached from the PLA matrix when the PLA matrix ruptured. It is hypothesized that a decrease in the filler–matrix interactions with an increasing HNT concentration could facilitate the hydrogen bonds breaking between the HNT aggregates and the PLA matrix, due to the increased phase separation and HNT aggregation. The SEM micrographs revealed a uniform dispersion of HNTa [Figure 5(c,e)] as compared with that of unmodified HNT [Figure 5(b,d)]. HNTa shows a much better dispersion in the PLA matrix than HNT, which is due to more hydrogen bonding between the HNTa and the PLA. Thus, the PLA/HNTa nanocomposites show high mechanical properties than the PLA/HNT nanocomposites.

Mechanical Properties

Figure 6 exhibits the stress-stain curves of pure PLA, PLA/HNT, and PLA/HNTa composites. The effect of reinforcement was shown in PLA/HNTa composites, however, there was no reinforcement effect for the PLA/HNT composites due to poor interface interaction between unmodified HNT and PLA matrix. Figure 7 shows the influence of the HNT or HNTa on the mechanical properties of the PLA. Both nanofillers effectively improved the modulus of the PLA. For example, the moduli of the 9PHNT and 9PHNTa nanocomposite are 3690 and 3789 MPa, which are ca. 25 and 28% higher than that of the pristine PLA, respectively. Both the nanocomposites show a lower elongation at break (Eb) than that of the pristine PLA, which is

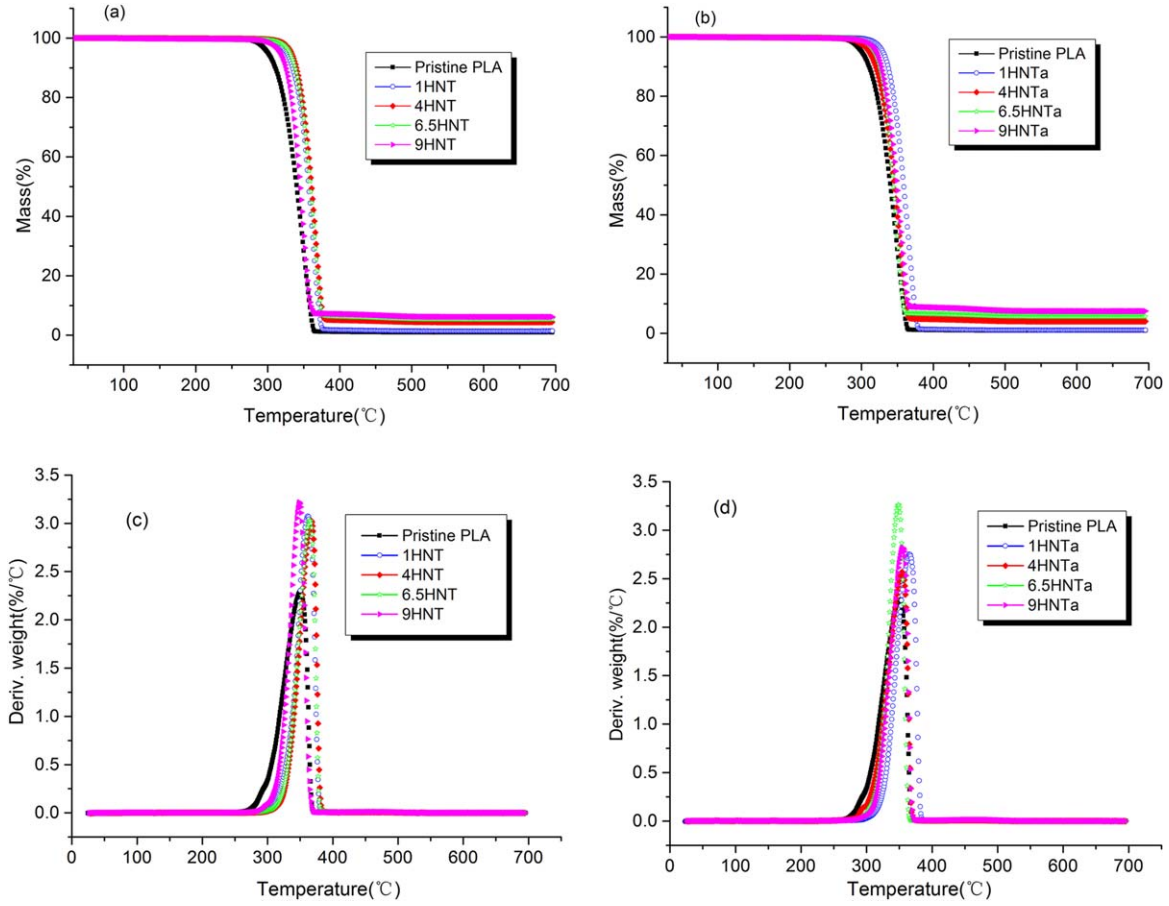

Figure 8. TGA curves of (a) pristine PLA and PLA/HNT nanocomposites, (b) pristine PLA and PLA/HNTa nanocomposites, and DTG curves of (c) pristine PLA and PLA/HNT nanocomposites, (d) pristine PLA and PLA/HNTa nanocomposites. [Color figure can be viewed at wileyonlinelibrary.com.]

ascribed to the addition of the rigid nanofillers in the PLA matrix. It is well known that the addition of stiff reinforcements can reduce the elongation of break of the matrix due to stress concentrations. The tensile strength of the PLA/HNT nanocomposites decreased with the addition of the HNTs. However, for the PLA/HNTa composites, the tensile strength increased with an increased loading of HNTa. Furthermore, the tensile strength of PLA/HNTa (9 wt %) composites is 81.9 MPa, which increases by 10.5% compared to pristine PLA. This reinforcing effect on the PLA arises from the structural characteristics of the nanoparticles, the dispersion state, and the interfacial interactions in these systems. It was shown that the treatment of

Table III. TGA Data of Pristine PLA, PLA/HNT Nanocomposites, and PLA/HNTa Nanocomposites

Entry	Sample	$T_{5\%}$ (°C)[a]	$T_{50\%}$ (°C)[a]	$T_{90\%}$ (°C)[a]	T_d (°C)[a]	Residue (%) (at 700 °C)
1	PLA	300.7	339.7	357.7	350.7	0.94
2	1PHNT	326.5	356.7	370.3	361.9	1.40
3	4PHNT	333.0	361.5	374.9	367.0	4.39
4	6.5PHNT	333.9	359.0	372.9	365.5	5.38
5	9PHNT	337.9	355.5	369.9	368.9	6.15
6	1PHNTa	310.9	344.5	354.3	355.4	1.06
7	4PHNTa	315.6	345.6	362.3	354.0	4.09
8	6.5PHNTa	320.8	346.6	359.6	358.9	5.69
9	9PHNTa	330.1	349.7	364.9	365.5	7.50

[a]$T_{5\%}$, $T_{50\%}$, and $T_{90\%}$ represent temperature of 5%, 50%, 90% weight loss, respectively. T_d represents temperature of the maximum rate of degradation.

HNT with NaOH helps to retain better values of T_s, which is mainly ascribed to the uniform distribution of alkalized halloysites in the PLA matrix.

Thermal Stability

TGA measurements were conducted to study the effect of HNT and HNTa on the thermal stability of the nanocomposites, and the TGA and DTG curves are shown in Figure 8. For simplification, Table III summarizes TGA data including the temperature of 5, 50, and 90% weight loss ($T_{5\%}$, $T_{50\%}$, and $T_{90\%}$), temperature of the maximum rate of degradation (T_d) and residue for each sample. The $T_{5\%}$ is often considered as the initial decomposition temperature. The pristine PLA almost degraded completely, while the PLA/HNT composites left some residues related to the HNT. The 1PHNT nanocomposite showed a higher thermal stability ($T_{5\%}$, 326.5 °C) compared to the pristine PLA ($T_{5\%}$, 300.7 °C). Furthermore, $T_{5\%}$ of the nanocomposites increased with the loading of HNT and HNTa. The PLA/HNTa composites showed lower $T_{5\%}$ values than the PLA/HNT composites due to the detachment of hydroxyl groups on the external surface of the HNTa. Furthermore, temperature at 50% weight loss ($T_{50\%}$), temperature at 90% weight loss ($T_{90\%}$), and temperature of the maximum rate of degradation (T_d) were improved with the loading of the nanofillers. However, the PLA/HNTa nanocomposites showed lower T_d compared to the PLA/HNT composites with the same loading of nanofillers. The residue at 700 °C increased with an increasing loading of the HNTa. The increased thermal stability of the PLA/HNTa nanocomposites could be attributed to the fact that the dispersed HNTa in the PLA matrix has a barrier effect on the volatile pyrolyzed products of PLA, eventually retarding the thermal degradation of the nanocomposites.

CONCLUSIONS

Alkalized treatment of halloysite is testified to be a facile and effective method to improve the dispersion of HNTs in the PLA matrix. More hydrogen bondings were formed between the hydroxyl groups of PLA molecules and alkalized HNT than unmodified HNT, which improved the interfacial interaction of PLA matrix and alkalized HNT. Alkalized HNT could act as a nucleating agent for PLA, which leads to decreased cold crystallization temperature and increased crystallinity. Alkalized HNT significantly increases the modulus and tensile strength of PLA, due to the better dispersion of HNTa in the PLA matrix than unmodified HNT. The thermal analyses evidence some increasing in PLA thermal stability with the addition of alkalized HNTs as compared with the pristine PLA.

ACKNOWLEDGMENTS

This work was supported by the National Natural Science Foundation of China under Grants Nos. 11374066 and 51103048 and the Fundamental Research Funds for the Central Universities under Grant No. 2014ZZ0007. The authors would like to thank Dr. Ma and Mr. William Tait for their help on revising this manuscript.

REFERENCES

1. Gorrasi, G.; Pantani, R.; Murariu, M. *Macromol. Mater. Eng.* **2014**, *299*, 104.
2. Silva, R. T. D.; Pasbakhsh, P.; Mae, L. S. *Appl. Clay Sci.* **2015**, *111*, 10.
3. Nampoothiri, K. M.; Nair, N. R.; John, R. P. *Bioresour. Technol.* **2010**, *101*, 8493.
4. Murariu, M.; Bonnaud, L.; Yoann, P.; Fontaine, G.; Bourbigot, S.; Dubois, P. *Polym. Degrad. Stab.* **2010**, *95*, 374.
5. Murariu, M.; Ferreira, A. D.; Alexandre, M.; Dubois, P. *Polym. Adv. Technol.* **2008**, *19*, 636.
6. Yang, T. C.; Hung, K. C.; Wu, T. L.; Wu, T. M.; Wu, J. H. *Polym. Degrad. Stab.* **2015**, *121*, 230.
7. Solarski, S.; Ferreira, M.; Devaux, E.; Fontaine, G.; Bachelet, P.; Bourbigot, S.; Delobel, R.; Coszach, P.; Murariu, M.; Ferreira, A. D. S.; Alexandre, M.; Degee, P.; Dubois, P. *J. Appl. Polym. Sci.* **2008**, *109*, 841.
8. Silva, R. T. D.; Pasbakhsh, P.; Goh, K. L.; Chai, S. P.; Chen, J. *J. Compos. Mater.* **2014**, *48*, 3705.
9. Bourbigot, S.; Fontaine, G.; Gallos, A.; Bellayer, S. *Polym. Adv. Technol.* **2011**, *22*, 30.
10. Pluta, M. *Polymer* **2004**, *45*, 8239.
11. Murariu, M.; Doumbia, A.; Bonnaud, L.; Dechief, A. L.; Paint, Y.; Ferreira, M.; Campagne, C.; Devaux, E.; Dubois, P. *Biomacromolecules* **2011**, *12*, 1762.
12. Du, M. L.; Guo, B. C.; Jia, D. M. *Polym. Int.* **2010**, *59*, 574.
13. Gorrasi, G.; Bugatti, V.; Vittoria, V. *Carbohydr. Polym.* **2012**, *89*, 132.
14. Zenkiewicz, M.; Richert, J. *Polimery* **2009**, *54*, 299.
15. Piekarska, K.; Sowinski, P.; Piorkowska, E.; Haque, M. M.-U.; Pracella, M. *Compos. Part A Appl. Sci. Manufac.* **2016**, *82*, 34.
16. Huang, H. D.; Ren, P. G.; Xu, J. Z.; Xu, L.; Zhong, G. J.; Hsiao, B. S.; Li, Z. M. *J. Memb. Sci.* **2014**, *464*, 110.
17. Deng, S. Q.; Zhang, J. N.; Ye, L.; Wu, J. S. *Polymer* **2008**, *49*, 5119.
18. Liu, M. X.; Guo, B. C.; Du, M. L.; Cai, X. J.; Jia, D. M. *Nanotechnology* **2007**, *18*, 455703.
19. Liu, M. X.; Zhang, Y.; Zhou, C. R. *Appl. Clay Sci.* **2013**, *75–76*, 52.
20. Rawtani, D.; Agrawal, Y. K. *Rev. Adv. Mater. Sci.* **2012**, *30*, 282.
21. Silva, R. T. D.; Pasbakhsh, P.; Goh, K. L. *Polym. Test.* **2013**, *32*, 265.
22. Jamaludin, N. A.; Inuwa, I. M.; Hassan, A. *J. Appl. Polym. Sci.* **2015**, *132*, DOI: 10.1002/app.42608.
23. Lecouvet, B.; Gutierrez, J. G.; Sclavons, M.; Bailly, C. *Polym. Degrad. Stab.* **2011**, *96*, 226.
24. Pasbakhsh, P.; Ismail, H.; Fauzi, M. N. A.; Bakar, A. A. *Appl. Clay Sci.* **2010**, *48*, 405.
25. Rybinski, P.; Pajak, A.; Janowska, G. *J. Appl. Polym. Sci.* **2015**, *132*, DOI: 10.1002/app.42593.

26. Zeng, S. S.; Reyes, C.; Liu, J. J.; Rodgers, P. A.; Wentworth, S. H.; Sun, L. Y. *Polymer* **2014**, *55*, 6519.
27. Fischer, E. W.; Sterzel, H. J.; Wegner, G. Kolloid-Z.u.Z. *Polymere* **1973**, *251*, 980.
28. Siracusa, V. *Int. J. Polym. Sci.* **2012**, *2012*, 302029.
29. Wu, C. S.; Liao, H. T. *Polymer* **2007**, *48*, 4449.
30. Papageorgiou, G. Z.; Achilias, D. S.; Nanaki, S.; Beslika, T.; Bikiaris, D. *Thermochim. Acta* **2010**, *511*, 129.
31. Pantani, R.; Santis, F. D.; Sorrentino, A.; Maio, F. D.; Titomanlio, G. *Polym. Degrad. Stab.* **2010**, *95*, 1148.
32. Rooj, S.; Das, A.; Thakur, V.; Mahaling, R. N.; Bhowmick, A. K.; Heinrich, G. *Mater. Des.* **2010**, *31*, 2151.
33. Peng, Y.; Southon, P. D.; Liu, Z. W. *J. Phys. Chem. C* **2008**, *112*, 15742.
34. Bocchini, S.; Fukushima, K.; Blasio, A. D.; Fina, A.; Frache, A.; Geobaldo, F. *Biomacromolecules* **2010**, *11*, 2919.